The pressure-temperature phase diagram of $(N(CH_3)_4)_2FeCl_4$ crystals: birefringent, elastic and electroacoustic properties

1993 J. Phys.: Condens. Matter 5 235

(http://iopscience.iop.org/0953-8984/5/2/011)

J. Phys.: Condens. Matter 5 (1993) 235–246. Printed in the UK

The pressure–temperature phase diagram of $\{N(CH_3)_4\}_2FeCl_4$ crystals: birefringent, elastic and electroacoustic properties

A V Kityk, V P Soprunyuk and O G Vlokh
Lviv State I Franko University, 1 Universitetska Street, 290602 Lviv, Ukraine

Received 15 April 1992

Abstract. The influence of the hydrostatic pressure on the temperature dependences of the ultrasonic velocities and attenuations, optical birefringence and electroacoustic coefficient f^*_{443} is studied in the vicinity of the phase transition temperatures of $\{N(CH_3)_4\}_2FeCl_4$ crystals. The pressure–temperature phase diagram is obtained. The results are discussed within the framework of phenomenological theory.

1. Introduction

Tetramethylammonium tetrachloroferrate (TMATC-Fe) $\{N(CH_3)_4\}_2FeCl_4$ belongs to the large group of A_2BX_4 crystals with the β-K_2SO_4-type structure in the high-temperature paraelastic (P) phase (space group, D^{16}_{2h}). On decrease in the temperature these crystals undergo four successive phase transitions (PTs): to the incommensurate (I) phase at $T_i = 282$ K with the structural modulation wavevector $k_0 = \xi a^*$, to the commensurate (C) modulated phase at $T_c = 270.5$ K (space group, D^4_2; $k_{c_1} = \frac{3}{7}a^*$), to the improper ferroelastic (IF) phase at $T_1 = 266.5$ K (space group, C^5_{2h}; $k_{c_2} = \frac{1}{3}a^*$) and, finally, to the proper ferroelastic (PF) phase at $T_2 = 240$ K (space group, C^5_{2h}; $k_{c_3} = 0$) (Mashiyama and Tanisaki 1982). The modulation parameter ξ in the I phase varies from 0.445 at T_i to 0.432 at T_c and then jumps to its commensurate value of $\frac{3}{7}$, which corresponds to the appearance of the C phase. The pressure–temperature (P–T) phase diagram in the temperature range 230–300 K and pressure range 0.1–200 MPa for TMATC-Fe crystals was previously obtained by dielectric and differential thermal analysis (DTA) measurements (Shimizu *et al* 1980, Gesi 1986). The new pressure-induced ferroelectric (F) phase (space group, C^9_{2v}; $k_{c_4} = \frac{2}{5}a^*$) was found at applied pressures between 20 and 70 MPa. The IF and I phases disappear at about $P_{k_4} = 100$ MPa and $P_{k_1} = 150$ MPa, respectively, and the direct PT from the P to the PF phase is observed at $P > P_{k_1}$.

In this paper we report the effect of hydrostatic pressure on the temperature behaviour of the acoustic and optical properties in the vicinity of PTs and triple points of TMATC-Fe crystals. The results obtained are discussed within the framework of the phenomenological theory. Similar measurements for the isostructural compounds TMATC-Zn, TMATC-Co and TMATC-Mn have been performed earlier (Vlokh *et al* 1989, 1990a, b, c).

2. Experimental procedures

Single crystals of TMATC-Fe were grown at about 300 K in a nitrogen atmosphere by a slow evaporation method from aqueous solution containing stoichiometric proportions of $N(CH_3)_4Cl$ and $FeCl_2$. The single crystals grown were of a good optical quality. The crystallographic axes were determined by the x-ray diffraction method. We use the next crystallographic orientation: $b = Y > a = X > c = Z$ ($b \simeq \sqrt{3}c$; a is the pseudo-hexagonal axis). The plane parallel specimens have typically a 4 mm × 4 mm × 5 mm size.

The temperature dependences of the optical birefringence ($\lambda = 632.8$ nm) were studied by Senarmonth's method with an accuracy of up to 10^{-7}. Velocity changes of the longitudinal and shear ultrasonic waves (USWs) ($f = 10$ MHz) were measured by the pulse-echo overlap method (Papadakiz 1967) with an accuracy of the order of 10^{-4}–10^{-5}. The accuracy of the absolute velocity determination was about 0.5%. The ultrasonic attenuation was determined from the decay rate of echo pulses with an accuracy of about 10%. Optical and acoustic investigations under an applied hydrostatic pressure have been performed in the ranges from 0.1 to 200 MPa and from 250 to 310 K using a high-pressure optical camera with a rate of temperature change of about 0.1 K min^{-1}.

3. Experimental results

The temperature dependences of the optical birefringence along the c axis of TMATC-Fe at different pressures are shown in figure 1. At the normal pressure ($P = 0.1$ MPa) the temperature dependence of birefringence changes $\delta(\Delta n_c)$ shows a clear anomalous behaviour in the vicinity of the P–I and C–IF PTs. In particular, a discontinuity near T_1 and a kink in the curve at T_i are observed, which corresponds to the first- and second-order PTs, respectively. Near the I–C PT, only a weak kink in the $\delta(\Delta n_c)$ temperature dependence is observed. Under an applied hydrostatic pressure the temperatures of the P–I and C–IF PTs shift to the high-temperature region. At high pressures a strong jump and clear kink in the $\delta(\Delta n_c)$ temperature dependence appear in the vicinity of the I–PF and P–PF PTs, respectively.

The temperature dependences of the longitudinal USW velocity V_3($\boldsymbol{q}\|c$, and $\boldsymbol{E}\|c$, where $\boldsymbol{q}$ is the wavevector of the USW and $\boldsymbol{E}$ is its polarization) for TMATC-Fe crystals at different pressures are shown in figure 2. At $P = 0.1$ MPa a clear decrease in velocity V_3 in the vicinity of T_i and its jump-like increase at T_1 are observed. The PT from P to I phase is also accompanied by anomalous attenuation of this USW (figure 2, inset). At high pressures, a sharp decrease in V_3 appears in the regions of the IF–PF, I–PF and P–PF PTs.

The temperature behaviour of the shear USW velocity V_4($\boldsymbol{q}\|c$ and $\boldsymbol{E}\|b$) (figure 3) at atmospheric pressure is similar to the corresponding behaviour for TMATC-Zn and TMATC-Co (Vlokh *et al* 1989, 1990b). On decrease in the temperature the velocity of this USW in the I phase firstly increases slightly and then essentially decreases. A kink in the $V_4(T)$ curve at T_c and a discontinuity in V_4 near T_1 occur in the region of the I–C and C–IF PTs, respectively. A decrease in the USW velocity V_4 in the I phase is accompanied by an attenuation increase (figure 3, inset (a)). Under an applied hydrostatic pressure the temperature changes in the USW velocity and attenuation in the I phase become sharper. At high pressures the IF–PF and I–PF

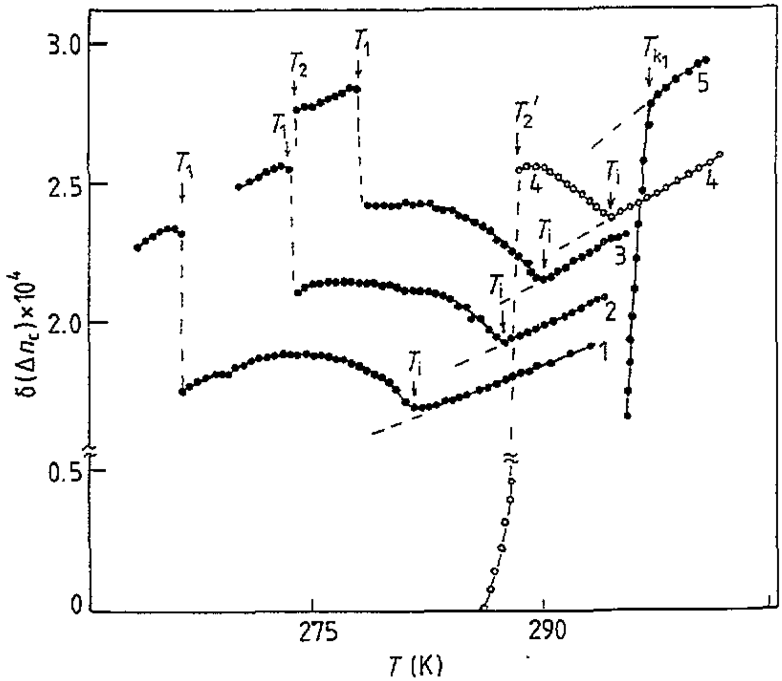

Figure 1. The temperature dependence of the optical birefringence of TMATC-Fe crystals at different pressures P: curve 1, 0.1 MPa; curve 2, 50 MPa; curve 3, 80 MPa; curve 4, 120 MPa; curve 5, 150 MPa. The PT temperatures indicated in this and subsequent figures can be understood by reference to the P–T phase diagram (figure 7).

PTs are accompanied by jumps in the value of V_4. At $P > 150$ MPa, only one kink in the $V_4(T)$ dependence occurs in the vicinity of the P–PF PT. Using the $V_4(T)$ dependences obtained at low pressures (figure 4), the region of existence of the C phase in the P–T phase diagram was determined. Under an applied hydrostatic pressure this phase disappears at the critical point ($P_{k_2} = 10$ MPa; $T_{k_2} = 273.5$ K) (see figure 7).

Figure 5 shows the temperature dependences of the USW velocity $V_6(q\|a$ and $E\|b)$ and anomalous attenuation $\Delta\alpha_6$ at different pressures. In the P phase the velocity V_6 is almost not changed on decrease in the temperature, but in the I phase a sharp decrease appears. A strong USW attenuation complicates the acoustic investigation in the C phase. Near the C–IF, IF–PF and I–PF PTs similar jump-like increases in V_6 are observed. At $P > P_{k_1}$, only a kink in the $V_6(T)$ dependence occurs in the region of the P–PF PT. The anomalous attenuation $\Delta\alpha_6$ at $P = 0.1$ MPa appears below T_i and increases on decrease in the temperature (figure 5, inset). Under an applied hydrostatic pressure the anomaly in $\Delta\alpha_6(T)$ for the I phase is gradually damped.

The temperature dependences of the shear USW velocity $V_5(q\|a$ and $E\|c)$ of TMATC-Fe crystals possess an anomalous temperature behaviour in the regions of almost all PTs (figure 6). The temperature changes in V_5 and $\Delta\alpha_5$ in the P and I phases become sharper under an applied hydrostatic pressure. The latter is very clearly observed at pressures close to P_{k_1}, where the anomalous decrease in V_5

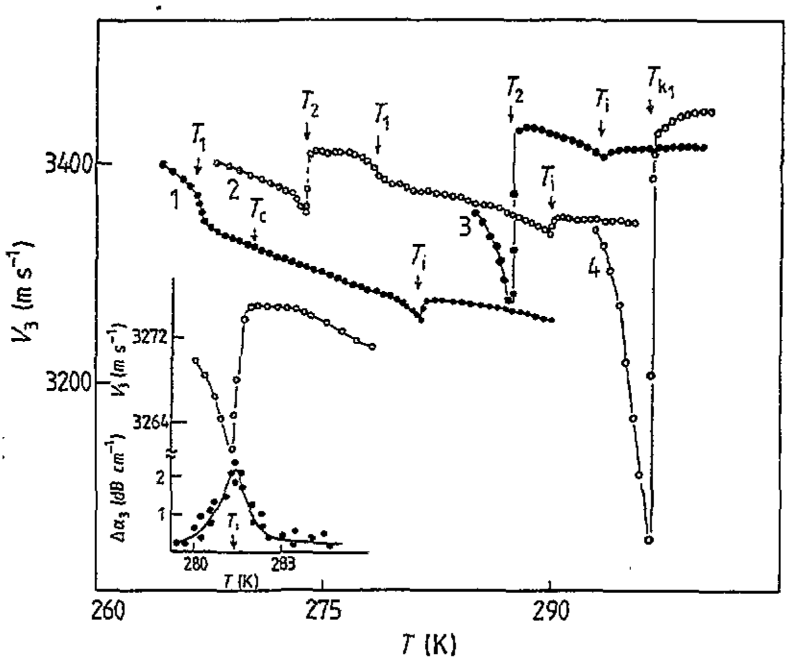

Figure 2. The temperature dependence of the longitudinal USW velocity V_3 at different hydrostatic pressures P: curve 1, 0.1 MPa; curve 2, 80 MPa; curve 3, 120 MPa; curve 4, 150 MPa. The inset shows the temperature dependences of the velocity V_3 and attenuation $\Delta\alpha_3$ in the vicinity of the P–I PT.

and increase in $\Delta\alpha_5$ occur in the region of the PT temperatures $T_i(P < P_{k_1})$ and $T_0(P > P_{k_1})$.

The P–T phase diagram obtained from the acoustic and optical measurements (figure 7) is in good agreement with the data on dielectric and DTA measurements (Shimizu *et al* 1980). The region of existence of the F phase in the P–T phase diagram was determined using the results of a linear electroacoustic effect (LEAE) investigation. Figure 8 shows the temperature dependences of the LEAE effective coefficient $f^*_{443} = f_{23233}/2C_{2323} = \Delta V_4/V_4E_3$ ($C_{2323} = C_{44}$ is the elastic modulus and E_3 the applied electric field) at different pressures. Appreciable changes in the USW velocity V_4 under an applied electric field along the c axis are observed at pressures between 15 and 75 MPa, where the F phase appears.

4. Discussion

The explanation of the anomalous temperature dependences of the optical birefringence at the PT to the I phase is straightforward. Following phenomenological Landau theory, the anomalous changes in the optical birefringence below T_i are proportional to the square of the order parameter amplitude Q_* (Konac 1979):

$$\delta(\Delta n_c) \sim Q_*^2 \sim (T_i - T)^{2\beta} \tag{1}$$

where β is the critical exponent. The experimental dependences of $\delta(\Delta n_c(T))$ in the region of the P–I PT are in good agreement with (1). At $P = 0.1$ MPa the critical

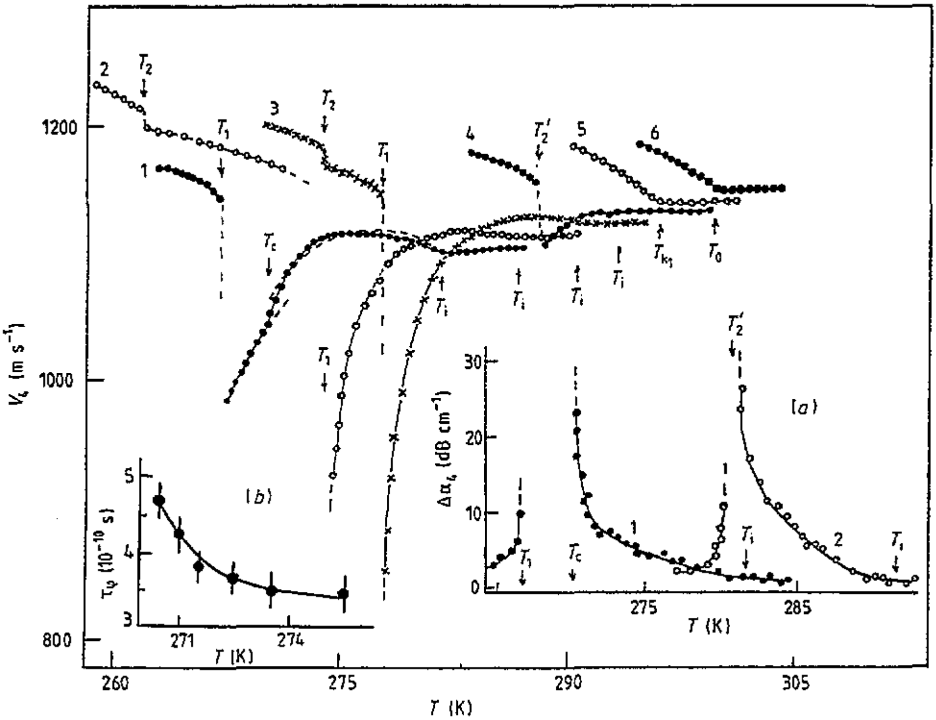

Figure 3. The temperature dependence of the shear USW velocity V_4 at different hydrostatic pressures P: curve 1, 0.1 MPa; curve 2, 50 MPa; curve 3, 80 MPa; curve 4, 120 MPa; curve 5, 150 MPa; curve 6, 168 MPa. Inset (*a*) shows the temperature dependence of the anomalous attenuation $\Delta\alpha_4$ at different hydrostatic pressures P: curve 1, 0.1 MPa; curve 2, 100 MPa. Inset (*b*) shows the temperature dependence of the non-Goldstone phason relaxation time τ_φ ($P = 0.1$ MPa).

exponent β is equal to 0.35 ± 0.02 which is close to the value obtained from x-ray measurement ($\beta \simeq 0.36$) (Mashiyama and Tanisaki 1982).

The temperature changes in the optical birefringence in the high-pressure region near the PT temperatures T_2' and T_0 may be explained in a similar way when we consider that $Q_* \to Q_0$, where Q_0 is the order parameter of the PF phase.

In the framework of phenomenological Landau theory the anomalous behaviours of the USW velocity and attenuation in the region of PTs are commonly explained on the basis of a free-energy expansion with the coupling terms, which correspond to anharmonic interactions between the strains U_1–U_6 and the order parameter. It is convenient to use as order parameter the normal phonon coordinate Q_k which belongs to the irreducible representation Σ_3 of the space group symmetry of the high-temperature P phase. According to Mashiyama (1980) the free energy can be written as

$$F = F_Q + F_{Q,U}$$

$$F_Q = \omega_k^2 Q_k^* Q_k + \tfrac{1}{2} B (Q_k^* Q_k)^2 + \tfrac{1}{3} C (Q_k^* Q_k)^3 + \dots$$

$$F_{Q,U} = \sum_{i=1}^{3} a_i Q_k^* Q_k U_i + \tfrac{1}{2} \sum_{i=1}^{6} b_i Q_k^* Q_k U_i^2 + \beta_0 Q_0 U_5 + \beta_5 (Q_{2/5}^5 + Q_{2/5}^{*5}) U_5 \qquad (2)$$

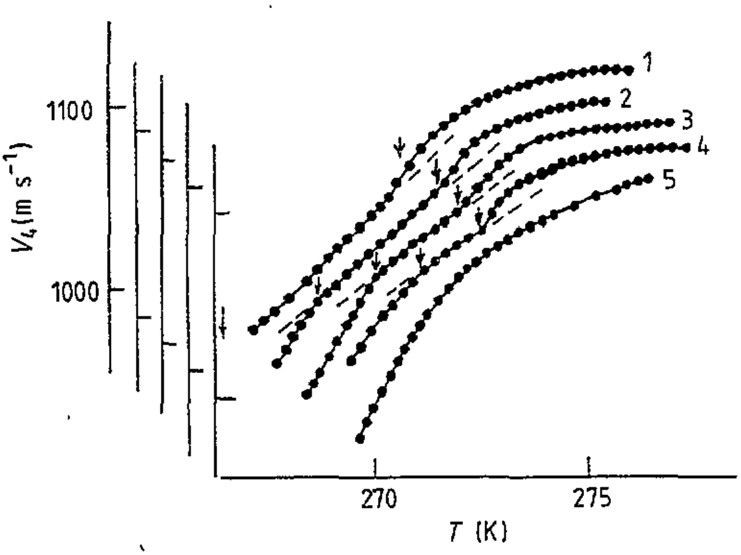

Figure 4. The V_4 temperature dependences in the region of existence of the C phase at different hydrostatic pressures P: curve 1, 0.1 MPa; curve 2, 3.2 MPa; curve 3, 5.5 MPa; curve 4, 7.5 MPa; curve 5, 10 MPa. The region of the C phase is marked by arrows.

$$+ \beta_3(Q_{1/3}^3 + Q_{1/3}^{*3})U_4 + \beta_7(Q_{3/7}^7 + Q_{3/7}^{*7})U_4$$
$$+ \beta_2^* Q_{k_0}^2 U_6(K') + \beta_3^* Q_{k_0}^3 U_4(K'')$$

where $\omega_k^2 = A_0(T - T_i) + h(k_0 - k)^2$ is the soft-mode frequency squared, $K' = a^* - 2k_0$, $K'' = a^* - 3k_0$, and Q_{k_0}, $Q_{3/7}$, $Q_{2/5}$, $Q_{1/3}$ and Q_0 are the normal-mode coordinates in the I, C, F, IF and PF phases, respectively. In the following only the lowest-order terms ($n = 2$, 3 and 4) are considered. As has been shown by Dvorak and Esayan (1982) and Lemanov and Esayan (1987), for the wavevector $q \ll K'(K'')$ of the USW the last two terms in (2) may be written as

$$\beta_2^* Q_{k_0}^* R_{k_0+q} U_6(q) \qquad \beta_3^* Q_{k_0}^2 Q_{a^*-2k_0+q} U_4(q) \tag{3}$$

where R_{k_0+q} and $Q^*_{a-2k_0+q}$ are the changes in the upper-mode and second-harmonic modulation normal-mode coordinates under the action of the V_6 and V_4 USWs, respectively. Using the normal-mode coordinates of the soft-mode amplitudon and phason (Dvorak and Petzelt 1978) it is possible to express the changes in the complex elastic modulus in the I phase (see, e.g., Rehwald *et al* (1980) and Lemanov and Esayan (1987)) as

$$\Delta C_{ii}^* = b_i Q_*^2 - 2\alpha_i^2 Q_*^2/\omega_A^2(q)[1 + i\Omega\tau_A(q)] \qquad i = 1,2,3$$
$$\Delta C_{44}^* = b_4 Q_*^2 - \tfrac{1}{2}\beta_3^{*2} Q_*^4\{1/\omega_A^2(K'')[1 + i\Omega\tau_A(K'')]$$
$$+ 1/[\omega_\varphi^2(K'')(1 + i\Omega\tau_\varphi(K'')]\} \tag{4}$$
$$\Delta C_{55}^* = b_5 Q_*^2$$
$$\Delta C_{66}^* = b_6 Q_*^2 - 2\beta_2^{*2} Q_*^2/\omega_R^2(k_0)[1 + i\Omega\tau_R(k_0)]$$

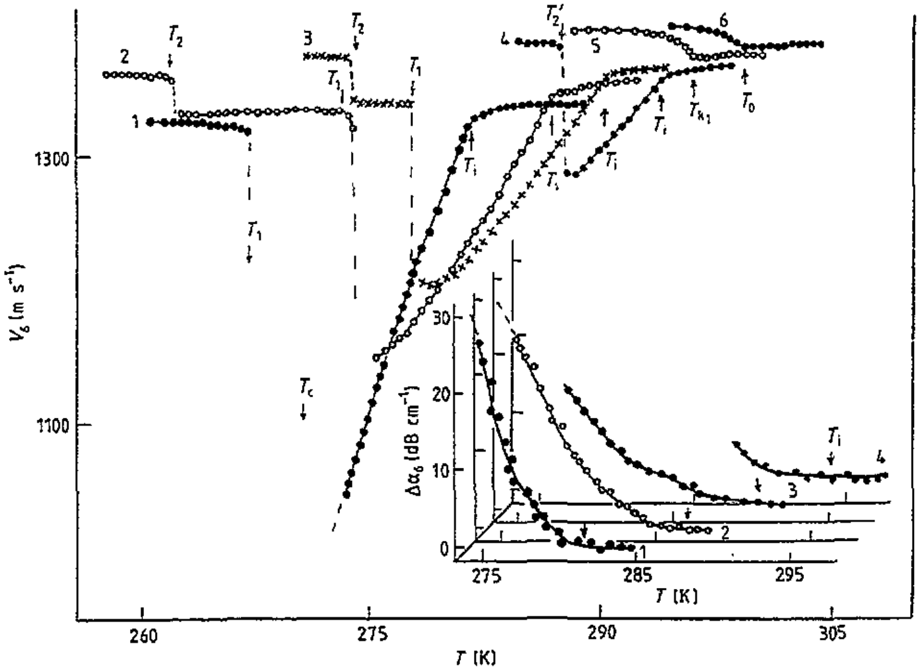

Figure 5. The temperature dependences of the shear USW velocity V_6 at different hydrostatic pressures P: curve 1, 0.1 MPa; curve 2, 50 MPa; curve 3, 80 MPa; curve 4, 120 MPa; curve 5, 150 MPa; curve 6, 168 MPa. The inset shows the temperature dependences of the anomalous attenuation $\Delta\alpha_6$ at different hydrostatic pressures P: curve 1, 0.1 MPa; curve 2, 50 MPa; curve 3, 80 MPa; curve 4, 120 MPa.

where $\Omega = qV$ is the USW frequency, $\omega_A^2(q) = 2A_0(T_i - T) + hq^2$ and $\tau_A(q)$ are the amplitudon frequency and relaxation time, respectively, $\omega_\varphi^2(K'') = hK''^2 = h[(3\xi - 1)a^*]^2$ and $\tau_\varphi(K'')$ are the non-Goldstone phason frequency and relaxation time, respectively, and $\omega_R(k_0)$ and $\tau_R(k_0)$ are the upper-mode frequency and relaxation time, respectively. Using the well known relations between changes in the complex elastic modulus ΔC_{ii}^*, ultrasonic velocities ΔV_i and attenuations $\Delta\alpha_i$ given by

$$\Delta V_i/V_i = \mathrm{Re}(\Delta C_{ii}^*)/2C_{ii} \qquad \Delta\alpha_i = \Omega\mathrm{Im}(\Delta C_{ii}^*)/2C_{ii} \tag{5}$$

we obtain, for changes in the longitudinal and shear USW velocities ΔV_i and attenuations $\Delta\alpha_i$,

$$\Delta V_3 = (1/2\rho V_3)[b_3 Q_*^2 - 2a_3^2 Q_*^2/\omega_A^2(1 + \Omega^2\tau_A^2)] \tag{6a}$$

$$\Delta\alpha_3 = (1/\rho V_3^2)[a_3^2 Q_*^2 \Omega^2 \tau_A/\omega_A^2(1 + \Omega^2\tau_A^2)] \tag{6b}$$

$$\Delta V_4 = (1/2\rho V_4)[b_4 Q_*^2 - \beta_3^{*2} Q_*^4/2\omega_\varphi^2(1 + \Omega^2\tau_\varphi^2)] \tag{7a}$$

$$\Delta\alpha_4 = (1/\rho V_4^2)[\beta_3^{*2} Q_*^4 \Omega^2 \tau_\varphi/4\omega_\varphi^2(1 + \Omega^2\tau_\varphi^2)] \tag{7b}$$

$$\Delta V_5 = (1/2\rho V_5) b_5 Q_*^2 \qquad \Delta\alpha_5 = 0 \tag{8}$$

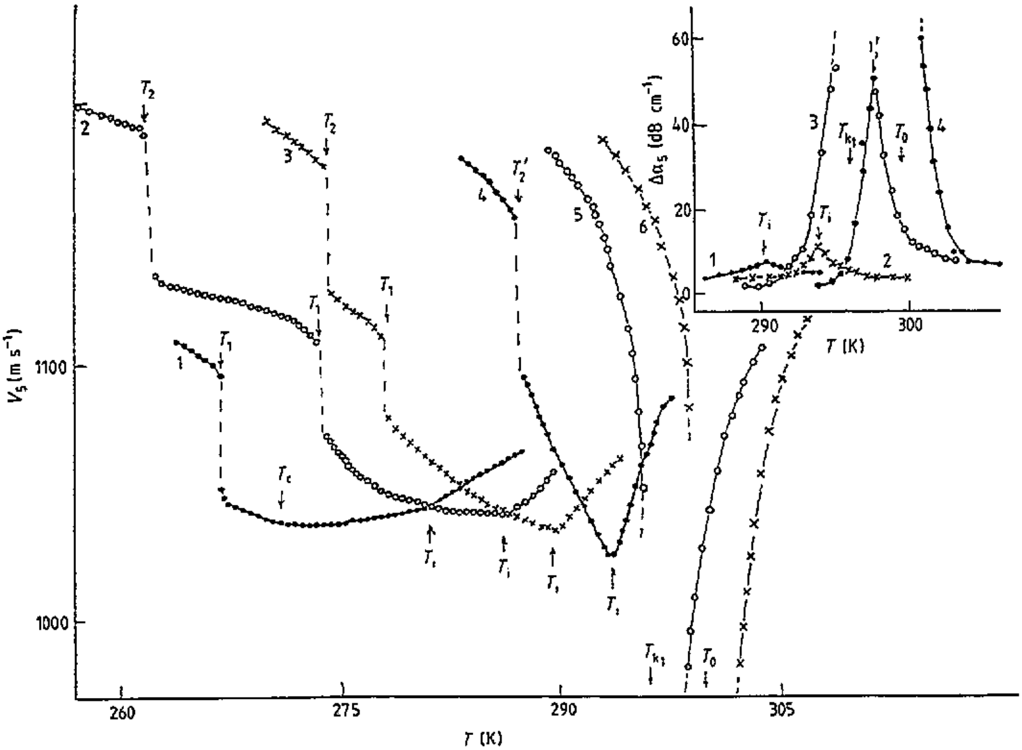

Figure 6. The temperature dependence of the shear USW velocity V_5 at different hydrostatic pressures P: curve 1, 0.1 MPa; curve 2, 50 MPa; curve 3, 80 MPa; curve 4, 120 MPa; curve 5, 150 MPa; curve 6, 168 MPa. The inset shows the temperature dependences of the anomalous attenuation $\Delta\alpha_5$ at different hydrostatic pressures P: curve 1, 80 MPa; curve 2, 120 MPa; curve 3, 150 MPa; curve 4, 168 MPa.

$$\Delta V_6 = (1/2\rho V_6)[b_6 Q_*^2 - 2\beta_2^{*2} Q_*^2/\omega_R^2(1+\Omega^2\tau_R^2)] \tag{9a}$$

$$\Delta\alpha_6 = (1/\rho V_6^2)[\beta_2^{*2} Q_*^2 \Omega^2 \tau_R/\omega_R^2(1+\Omega^2\tau_R^2)] \tag{9b}$$

where ρ is the crystal density. In (7a) and (7b), only the non-Goldstone phason contribution is considered since, according to Volkov *et al* (1980), $\omega_A \gg \omega_\varphi$.

It follows from (6a) that the value of the velocity V_3 should exhibit a sudden decrease at $T = T_i$, which is caused by the interaction between USWs and amplitudons. This is observed experimentally (figure 2). Using the experimental values of the negative velocity jump and anomalous attenuation, one can determine the amplitudon relaxation time. From the analysis of the experimental results it follows that $\tau_A = \tau^*/(T_i - T)$, where $\tau^* = 1 \times 10^{-9}$ s K. The changes in V_3 in the I phase are caused by the first term in (6a). In this way the temperature behaviour of V_3 in the vicinity of the PT temperatures T_2' and T_0 at high pressures can be explained if we consider that $Q_k \to Q_0$, $A_0 \to A_0'$, $B \to B'$, $b_3 \to b_3'$ and $a_3 \to a_3'$. The coupling coefficients of the free-energy expansion calculated from experimental data are presented in table 1.

The temperature changes in the shear USW velocities near the P–I PT are mainly caused by the first terms in (7a), (8) and (9a), which lead to the quadratic dependences

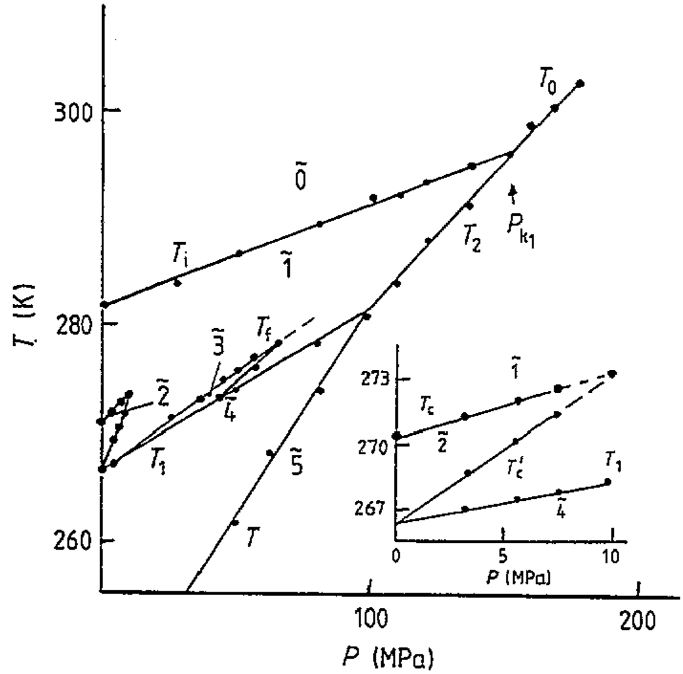

Figure 7. The P–T diagram of TMATC-Fe crystals: region $\tilde{0}$, P phase; region $\tilde{1}$, I phase; region $\tilde{2}$, C phase; region $\tilde{3}$, F phase; region $\tilde{4}$, IF phase; region $\tilde{5}$, PF phase. In the inset a more detailed C-phase region of the P–T diagram is shown.

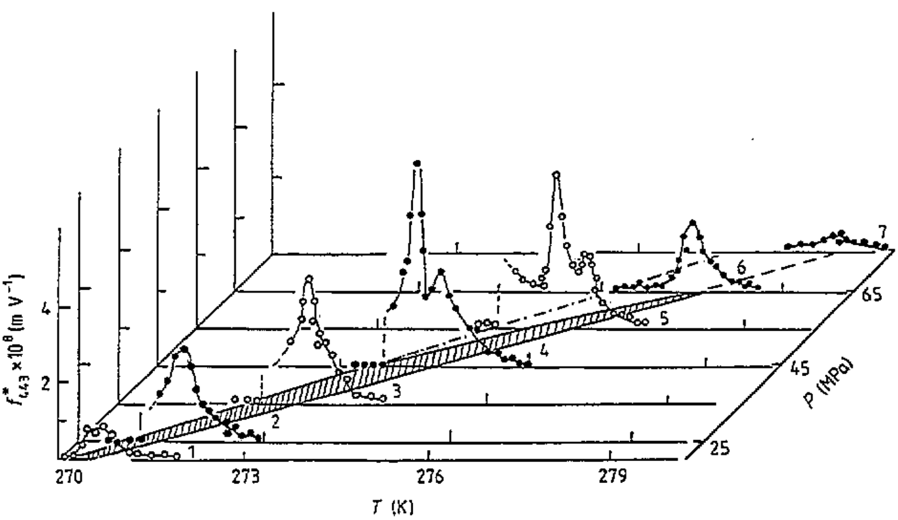

Figure 8. The temperature dependences of the LEAE effective coefficient f^*_{443} at different hydrostatic pressures P: curve 1, 20 MPa; curve 2, 25 MPa; curve 3, 35 MPa; curve 4, 45 MPa; curve 5, 55 MPa; curve 6, 65 MPa; curve 7, 75 MPa. The shaded part in the P–T plane corresponds to the region of the F phase.

of ΔV_i ($i = 4$–6) on the amplitude of the order parameter. Consequently, kinks in

Table 1. Coupling coefficients of the free-energy expansion.

P (MPa)	0.1	80	150
$a_3^2/B(10^8\ \mathrm{J\ m^{-3}})$	1.65	1.79	—
$a_3'^2/B'\ (10^8\ \mathrm{J\ m^{-3}})$	—	—	37.7
$b_3A_0/B\ (10^7\ \mathrm{J\ m^{-3}\ K^{-1}})$	7.9	6.9	—
$b_3'A_0'/B'\ (10^7\ \mathrm{J\ m^{-3}\ K^{-1}})$	—	—	93.4
$b_4A_0/B\ (10^7\ \mathrm{J\ m^{-3}\ K^{-1}})$	5.02	—	—
$b_4'A_0'/B'\ (10^7\ \mathrm{J\ m^{-3}\ K^{-1}})$	—	—	2.8
$b_5A_0/B\ (10^7\ \mathrm{J\ m^{-3}\ K^{-1}})$	1.04	3.1	—
$b_6A_0/B\ (10^7\ \mathrm{J\ m^{-3}\ K^{-1}})$	−9.9	−7.1	—
$b_6'A_0'/B'\ (10^7\ \mathrm{J\ m^{-3}\ K^{-1}})$	—	—	4.38
$\beta_3^{*2}A_0^2/B^2h\ (10^{25}\ \mathrm{J\ m^{-5}\ K^{-2}})$	4.89	—	—
$\beta_0^2/A_0'\ (10^9\ \mathrm{J\ K\ m^{-3}})$	—	—	1.15

$V_i(T)$ are observed at $T = T_i$. From the experimental data it follows that $b_4 > 0$, $b_5 > 0$ and $b_6 < 0$ (table 1).

The strong decrease in V_4 and increase in $\Delta\alpha_4$ with decreasing temperature are caused by the non-Goldstone phason contribution. This is due to the faster increase in Q_*^4/ω_φ^2 (at $\xi \to \frac{1}{3}$, $\omega_\varphi \to 0$) compared with Q_*^2. In contrast with TMATC-Mn (Vlokh *et al* 1990a) its influence on the elastic properties of TMATC-Fe appears even at atmospheric pressure, similarly to TMATC-Co and TMATC-Zn (Vlokh *et al* 1989, 1990b) crystals. We attribute this behaviour to the essentially lower-frequency value of the non-Goldstone phason mode, as the minimum of the soft mode of TMATC-Fe at $P = 0.1$ MPa is shifted to the $k = \frac{1}{3}a^*$ point, opposite to TMATC-Mn. The numerical calculation of the $V_4(T)$ dependence in the I phase (figure 3, dotted line) favours this conclusion, when taking into account the values of the corresponding expansion coefficients (table 1) and experimental data (Mashiyama and Tanisaki 1982). Using the velocity–temperature and attenuation–temperature dependences in the I phase and the relations (7*a*) and (7*b*) it is possible to determine the phason relaxation time. The temperature dependence of τ_φ is shown in figure 3, inset (*b*). Comparable calculations for high pressures have not been carried out since experimental data are not available. Simultaneously, under an applied hydrostatic pressure the negative contribution to the changes in ΔV_4 increases (figure 3), which indicates the strengthening of the non-Goldstone phason influence on the elastic properties. This behaviour is common for TMATC-Zn, TMATC-Co and TMATC-Mn crystals (Vlokh *et al* 1989, 1990a, b, c).

The temperature behaviour of the USW velocity V_6 in the I phase of TMATC-Fe at low pressures cannot be completely explained by the consideration of only the first term in (9*a*). The strong changes in this velocity are accompanied by the USW attenuation, whereas the coupling term $b_6 Q_k Q_k^* U_6^2$ does not induce anomalous attenuation, if we do not consider the order parameter fluctuation. Moreover, $\Delta V_6 \sim (T_i - T)^{2\beta}$, where $\beta \simeq 0.58$ essentially exceeds the critical exponent, obtained from optical birefringence and x-ray measurements (Mashiyama and Tanisaki 1982). Therefore the unusual temperature behaviour of the USW velocity V_6 and attenuation $\Delta\alpha_6$ in the low-pressure region may be explained correctly if we take into account the interaction between the USWs and the upper mode. The numerical calculation of the upper-mode contribution to the elastic properties is rather tedious, since it is difficult to estimate the temperature dependence of ω_R. With increasing pressure the k_0-value of the soft-mode condensation shifts from the Brillouin zone boundary to lower values and the frequency of ω_R increases. The latter is accompanied by the damping of the upper-mode contribution to the changes in USW attenuation and velocity in the I phase, which are in agreement with experimental data.

Let us discuss the temperature changes in the USW velocity V_5 and attenuation $\Delta\alpha_5$. In the free-energy expansion (2) the two coupling terms may explain the anomalous behaviours of $V_5(T)$ and $\Delta\alpha_5(T)$. At low pressures, when the PT temperature to the PF phase is far from the I phase, the variations in $\Delta V_5(T)$ and $\Delta\alpha_5(T)$ can be explained by (8), considering the $b_5 Q_k Q_k^* U_5^2$ coupling. In this case the $V_5(T)$ temperature dependence shows a kink at $T = T_i$ and an anomalous attenuation is absent. The typical changes in the V_5 temperature dependences at high pressures are caused by a significant increase in the role of the $\beta_0 Q_0 U_5$ coupling term. Elastic softening clearly appears in the region of the direct PT from the P to the PF phase, where the changes in V_5 are described by a Curie–Weiss law

$$\Delta V_5 = \begin{cases} (1/2\rho V_5)[\beta_0^2/A_0'(T-T_0)] & T > T_0 \\ (1/2\rho V_5)[\beta_0^2/2A_0'(T_0-T)] & T < T_0 \end{cases} \tag{10a}$$

and the anomalous attenuation by

$$\Delta\alpha_5 = \begin{cases} (1/2\rho V_5^2)[\beta_0^2\Omega^2\tau_0/(1+\Omega^2\tau_0^2)][1/A_0'(T-T_0)] & T > T_0 \\ (1/2\rho V_5^2)[\beta_0^2\Omega^2\tau_0/(1+\Omega^2\tau_0^2)][1/2A_0'(T_0-T)] & T < T_0 \end{cases} \tag{10b}$$

where τ_0 is the soft-mode relaxation time in the PF phase. The temperature dependences of V_5 and $\Delta\alpha_5$ observed near T_0 (figure 6) suggest the existence of the P–PF PT. The corresponding coupling coefficients in the free-energy expansion determined from the equation (10*a*) and experimental data (figure 6) are given in table 1.

The LEAE coefficients represent the components of the polar five-rank tensor. The P and IF phases both possess a centre of symmetry and consequently all $f_{ijklm} \equiv 0$. The LEAE is also not observed in the I phase, which indicates that the I phase is macroscopically centrosymmetrical. An analogous conclusion is obtained from the electro-optic (Vlokh *et al* 1984), optical second-harmonic generation (Sanctuary *et al* 1985, Esayan *et al* 1987) and optical activity (Vlokh *et al* 1985) measurements in similar I systems. The loss of the centre of symmetry in the F phase is accompanied by the appearance of the LEAE (figure 8). In this case the changes Δf_{443}^* in LEAE coefficient near the F–I PT ($T = T_f$) may be written in a form similar to that used by Agishev *et al* (1979):

$$\Delta f_{443}^* = (1/2C_{44})\{[\partial(\Delta C_{44}^{Q_*})/\partial T_f](\partial T_f/\partial E_3) + [\partial(\Delta C_{44}^{\varphi})/\partial\varphi](\partial\varphi/\partial E_3)\} \tag{11}$$

where $\Delta C_{44}^{Q_*}$ and ΔC_{44}^{φ} are the ΔC_{44} changes caused by the contribution of the order parameter amplitude Q_* and phase φ, respectively. In the framework of such considerations the anomalous behaviour of $f_{443}(T)$ can be related to the shift in the F–I PT temperature and change in phase φ under the applied electric field. A more detailed phenomenological analysis of (11) will be discussed in the future.

References

Agishev B A, Laichtman B D, Lemanov V V, Polchovskaya T M and Yushyn N K 1979 *Fiz. Tverd. Tela* **21** 142

Dvorak V and Esayan S Kh 1982 *Solid State Commun.* **44** 901
Dvorak V and Petzelt J 1978 *J. Phys. C: Solid State Phys.* **11** 4827
Esayan S Kh, Kityk A V and Lemanov V V 1987 *Sov. Phys.–Solid State* **29** 891
Gesi K 1986 *Ferroelectrics* **66** 269
Konak C 1979 *Phys. Status Solidi* a **54** 99
Lemanov V V and Esayan S Kh 1987 *Ferroelectrics* **73** 125
Mashiyama H 1980 *J. Phys. Soc. Japan* **49** 2270
Mashiyama H and Tanisaki S 1982 *J. Phys. C: Solid State Phys.* **15** L455
Papadakiz E P 1967 *J. Acoust. Soc. Am.* **42** 1045
Rehwald W, Vonlathen A, Kruger I K, Wallerius R and Unruh H G 1980 *J. Phys. C: Solid State Phys.* **13** 3823
Sanctuary R, Jund D, Baumelit J C and Gunter P 1985 *Phys. Rev.* B **32** 1649
Shimizu H, Abe N, Kokubo N, Yasuda N, Fujimoto S, Yamaguchi T and Sawada S 1980 *Solid State Commun.* **34** 363
Vlokh O G, Esayan S Kh, Kityk A V and Mokry O M 1989 *Bull. Acad. Sci. USSR, Phys. Ser.* **53** 130
Vlokh O G, Kityk A V and Mokry O M 1990a *Fiz. Tverd. Tela* **32** 1044
—— 1990b *Kristallografiya* **35** 894
—— 1990c *Fiz. Tverd. Tela* **32** 2558
Vlokh O G, Kityk A V and Polovinko I I 1984 *Sov. Phys.–Crystallogr.* **29** 703
—— 1985 *Sov. Phys.–Crystallogr.* **30** 1194
Volkov A A, Ishibashi Y, Kozlov G V and Petzelt J 1980 *Fiz. Tverd. Tela* **22** 1424